PAPER

Ethanol-sensing performance of tin dioxide octahedral nanocrystals with exposed high-energy {111} and {332} facets

Chenxia Wang, Daoping Cai, Bin Liu, Han Li, Dandan Wang, Yuan Liu, Lingling Wang, Yanrong Wang, Qiuhong Li* and Taihong Wang*

Tin dioxide octahedral nanocrystals with exposed high-energy {111} and {332} facets were hydrothermally synthesized and characterized by X-ray diffraction (XRD), scanning electron microscopy (SEM), transmission electron microscopy (TEM) and selected-area electron diffraction (SAED). Gas sensors were fabricated from the prepared SnO_2 nanocrystals and applied to ethanol-sensing tests. Octahedral SnO_2 {332} exhibited a maximum response of 2200 under an ethanol concentration of 800 ppm at 250 °C with a response time of 1.5 s and a recovery time of 32.5 s, whereas SnO_2 {111} exhibited a maximum response of 179 at 360 °C with a response time of 9.5 s and a recovery time of 6.7 s. The sensing mechanisms responsible for SnO_2 nanocrystals to ethanol vapor are discussed.

1   Introduction

Tin dioxide (SnO_2), an n-type semiconductor material with a wide band gap (3.6 eV, 27 °C), has a wide range of applications in areas such as dye-sensitized solar cells,[1,2] lithium battery,[3,4] and gas sensors, because SnO_2 exhibits better performance in semiconductors, particularly of optical and electrical characteristics. In particular, good properties for gas sensing with good response and recovery, long life, and low cost have made SnO_2 the best material in gas sensors. It is now fully accepted that a nanostructure adds value to material properties and diversifies the application areas.[5] SnO_2 nanoparticles can further improve gas sensing because of their small grain size, large surface-to-volume ratio, strong adsorption ability and high surface activity. Recently, several types of SnO_2 nanoparticles have been used to fabricate sensors for various gases such as nanoslabs,[6] nanotubes,[7] and nanowires.[8,9] In this work, SnO_2 octahedral nanocrystals with exposed high-energy {111} and {332} facets were used to fabricate sensors for ethanol sensing.

Presently, various shapes of SnO_2 nanostructures have been prepared by employing different techniques. For example, SnO_2 nanorods, nanosheets and nanoflowers have been synthesized by hydrothermal methods.[10–12] SnO_2 nanowires have been synthesized by hydrothermal[13] and thermal evaporation.[14] SnO_2 nanowire-mixed nanodendrites have been synthesized by carbothermal reduction.[15]

In principle, gas sensing by metal-oxide semiconductors such as SnO_2 is based on the oxidation–reduction reaction of the detected gases occurring on the semiconductor surface,

which leads to an abrupt change in the electrical conductance of the sensor.[16] Various surfaces have different geometric electronic structures, dangling bonds, and surface defects, which result in different physical and chemical properties. In this work, the properties of SnO_2 octahedral nanocrystals with exposed high-energy {111} and {332} facets were compared from the perspective of ethanol-sensing performance.

2   Experimental details

SnO_2 octahedral nanocrystals with exposed high-energy {111} and {332} facets were synthesized by a gentle and simple hydrothermal method. It should be mentioned that most wet chemical syntheses of SnO_2 nanoparticles are usually based on a hydrolytic process, which is highly sensitive to the pH of the reaction system. In this work, the high-energy {111} facets were controlled by regulating the basicity, whereas the high-energy {332} facets were controlled by regulating the acidity.

2.1   Synthesis of octahedral SnO_2 nanocrystals enclosed by {111} facets

The octahedral SnO_2 {111} nanocrystals were synthesized by hydrothermal synthesis.[17] In a typical process, 1 mmol $SnCl_4 \cdot 5H_2O$ (0.350 g) and 17 mL of 1 M aqueous tetramethyl-ammonium hydroxide (TMAH) were successively added to 3 mL of ethanol under intense ultrasonic treatment. Afterwards, the resulting solution was transferred to a Teflon-lined stainless-steel autoclave (25 mL) and maintained at 200 °C for 12 h. After cooling to room temperature, the white solids were collected by centrifugation and washed several times with deionized water and ethanol.

Pen-Tung Sah Institute of Micro-Nano Science and Technology, Xiamen University, Xiamen, China. E-mail: liqiuhong@xmu.edu.cn

This journal is © The Royal Society of Chemistry 2014

J. Mater. Chem. A, 2014, **2**, 10623–10628 | **10623**

2.2 Synthesis of octahedral SnO₂ nanocrystals enclosed by {332} facets

The octahedral SnO₂ {332} nanocrystals were synthesized using acid solution by hydrothermal synthesis.[18] In a typical synthesis, 1 mmol SnCl₂·2H₂O (0.225 g), 0.6 mL HCl, and 0.315 g polyvinyl pyrrolidone (PVP, K-30) were added sequentially to a mixed solvent of ethanol and distilled water (6 mL, 1 : 1 v/v) under intense ultrasonic treatment. The resulting solution was also transferred into a Teflon-lined stainless-steel autoclave (25 mL) and maintained at 200 °C for 12 h. Finally, another white solid was collected by the same method.

2.3 Sensor fabrication

The as-obtained SnO₂ octahedrals were mixed with a small amount of terpineol to form an SnO₂ paste, which was then brush coated onto the surfaces of Al₂O₃ microtubes with four Pt electrodes. After the coating was air dried, the SnO₂-coated Al₂O₃ microtube was fixed to a special pedestal with six poles by welding four Pt electrodes to four poles of the pedestal. An Ni–Cr heating coil was then inserted through the Al₂O₃ microtube, and its two ends were welded to the other two poles of the pedestal.

2.4 Ethanol-sensing measurements

The ethanol-sensing tests were conducted on a ZhongKe NS-4003 Smart Sensor Analyser (Beijing ZhongKe Micro-Nano Networking Technology Co., Ltd.). Ethanol as the detecting target was injected into a test container and mixed with air after complete evaporation. The concentration of ethanol vapor varied from 5 to 800 ppm, which was calculated according to the densities of ethanol and the volume of the testing container. The amounts (V_{tg}, μL) of ethanol were determined according to eqn (1).

$$V_{tg} = \frac{10^{-9} VMC_{tg}}{22.4\rho d}.$$ (1)

here, V, M, ρ and d denote the volume of the test container ($V = 10$ L), mole mass, density and rate of purity of the target liquid reagent ($M_{ethanol} = 46$ g mol⁻¹, $\rho_{ethanol} = 0.789$ g cm⁻³, $d_{ethanol} = 0.99$), respectively. C_{tg} denotes the concentration (ppm) of the target liquid reagent. The operating temperature was varied from 100 to 400 °C, and was controlled by setting the heating voltage from 2.5 to 5.5 V. The relative humidity (RH) of the environment was 40–50%.

An operating voltage of 2 V was loaded on the circuit. For the reducing gas of ethanol and the n-type semiconducting SnO₂ sensors, the response (S_r) is defined by eqn (2), where R_a and R_g are the resistances of the SnO₂ sensor in air and in ethanol ambient environments, respectively. R_a and R_g could be directly read in the report from the sensor analyser. The response time (T_{res}) is defined as the time required for the sensor to reach 90% of the stabilized value of its resistance in the presence of the test gas. Similarly, the recovery time (T_{rec}) is defined as the time required for the sensor to reach 10% of the initial steady-state value of its resistance after the gas was removed, which can be expressed as

$$S_r = R_a/R_g.$$ (2)

3 Results and discussion

The composition and phase of the as-prepared products were identified by X-ray diffraction (XRD) equipment (Rigaku Ultima IV XRD). The morphology and crystal structure of the as-prepared products were observed by scanning electron microscopy (SEM, S-4800) and transmission electron microscopy (TEM, JEM-2100) with an acceleration voltage of 200 kV. All the TEM samples were prepared by depositing a drop of diluted suspensions in ethanol on a carbon-film-coated copper grid. Fig. 1a and b show the typical XRD patterns of the as-prepared octahedral SnO₂ with exposed {111} and {332} facets, respectively, both of which can be indexed to the rutile phase of bulk SnO₂ with cell constants of $a = b = 4.7382$ and $c = 3.1871$ (PDF no. 00-041-1445). The SEM images of the as-prepared octahedral SnO₂ with exposed {111} and {332} facets are shown in Fig. 1c and d, respectively, indicating that both the products consist of high-purity particles with smooth surfaces. The size of the octahedral SnO₂ {111} is in the range of 150 to 250 nm (Fig. 1c), and the octahedral SnO₂ {332} particles have well-defined octahedral shapes, in which the edge-to-edge width (W) is about 95 nm and the apex-to-apex length (L) is around 140 nm (inset of Fig. 2b).

More detailed structural information on the octahedral SnO₂ was provided by TEM. Fig. 2a shows the TEM image and selected-area electron diffraction (SEAD) pattern (inset) of an octahedral SnO₂ {111} particle along the [2$\bar{2}$0] direction. The SEAD pattern confirmed that the particle has a single-crystal structure. As shown in Fig. 2a, the angles between the two side surfaces agree well with the model of octahedral SnO₂ with exposed {111} facets projected along the [2$\bar{2}$0] zone axis (Fig. 2b). In order to further confirm the exposed surfaces of the octahedral SnO₂, the same particle was rotated to the [1$\bar{1}\bar{1}$] zone axis from the [2$\bar{2}$0] zone axis. As shown in Fig. 2c and d, the angles of the particle still correspond well with the octahedral
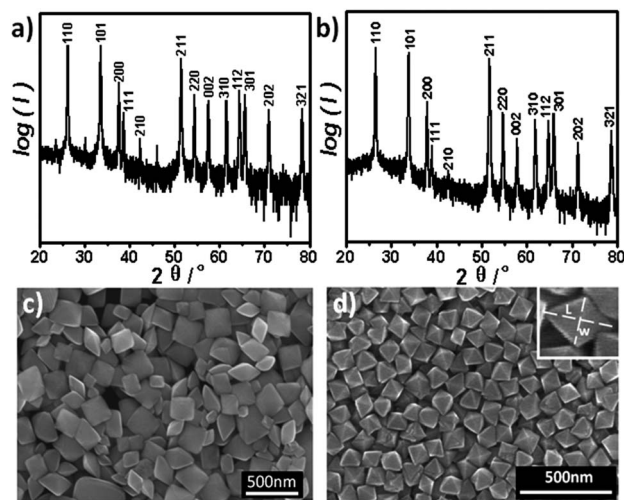

Fig. 1 (a) XRD pattern and (c) typical SEM image of octahedral SnO₂ {111}; (b) XRD pattern and (d) typical SEM image of octahedral SnO₂ {332}; inset: the corresponding magnified image.
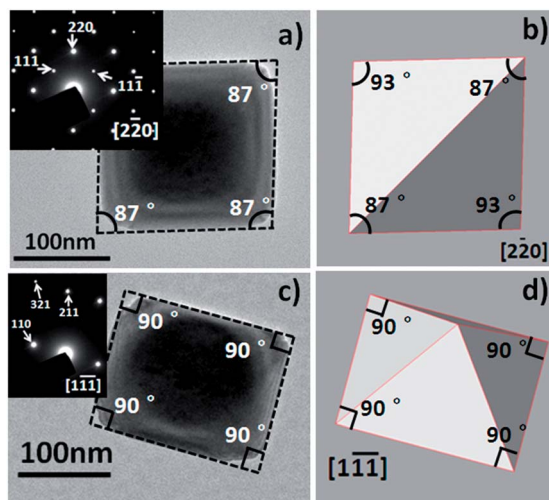
Fig. 2 (a) Typical TEM image of the octahedral SnO_2 {111} nanoparticle viewed along the [2$\bar{2}$0] direction; inset: the corresponding SEAD pattern. (b) Model of an ideal SnO_2 octahedron enclosed with {111} facets projected from the [2$\bar{2}$0] direction. (c) Typical TEM image of the octahedral SnO_2 {111} nanoparticle viewed along [1$\bar{1}\bar{1}$] direction; inset: the corresponding SEAD pattern. (d) Model of an ideal SnO_2 octahedron enclosed with {111} facets projected from the [1$\bar{1}\bar{1}$] direction.

SnO_2 model enclosed by {111} facets projected along the same direction. Therefore, it was concluded that the exposed surfaces of the first octahedral SnO_2 particle are {111} facets. The facets of the second octahedral SnO_2 particle were determined by the same method. Fig. 3a and c show the TEM images and SEAD patterns (inset) of an octahedral SnO_2 {332} particle along the
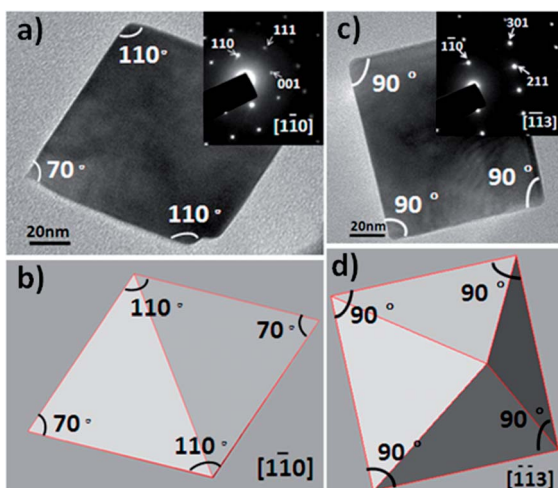
[1$\bar{1}$0] and [$\bar{1}\bar{1}$3] direction, respectively. Accordingly, Fig. 3b and d show the model of an ideal SnO_2 octahedron enclosed with {332} facets projected from the [1$\bar{1}$0] and [$\bar{1}\bar{1}$3] direction. As shown in the figure, the angles between the two side surfaces agree well with the model along two directions. Thus, it was concluded that the exposed surfaces of the second octahedral SnO_2 particle are {332} facets.

The as-obtained octahedral SnO_2 with exposed {111} and {332} facets were used to fabricate sensors (Fig. 4a). For the gas-sensing study, the operating temperature is important for the investigation of gas-sensing properties because of its significant influence on the surface state of sensing materials as well as the contact reactions during the gas-sensing process. Fig. 4b shows the responses of the two sensors based on SnO_2 {332} and {111} as a function of the operating temperature under an ethanol concentration of 800 ppm. As shown in the figure, the response of each sensor is strongly dependent on the operating temperature. With the temperature increasing from 100 to 400 °C, each sensor has an optimal operating temperature at which the sensor exhibits the highest response to ethanol. It can be found that the SnO_2 {111}-based sensor shows a maximum response of 179 at 360 °C, whereas the SnO_2 {332}-based sensor shows the maximum response of 2200 at 250 °C, which is 12 times higher than {111}. The response of the SnO_2 {332}-based to ethanol vapor is almost stronger than SnO_2 {111} at any other temperature except 400 °C, at which the response of SnO_2 {111} is slightly larger than SnO_2 {332}. Fig. 4c and d shows the response and recovery time of sensors based on SnO_2 {332} and {111} at different operating temperatures. The response time of the octahedral SnO_2 {111}-based sensor with an ethanol concentration of 800 ppm at temperatures varying from 100 to 400 °C are all below 35 s (Fig. 4c), whereas the duration of SnO_2
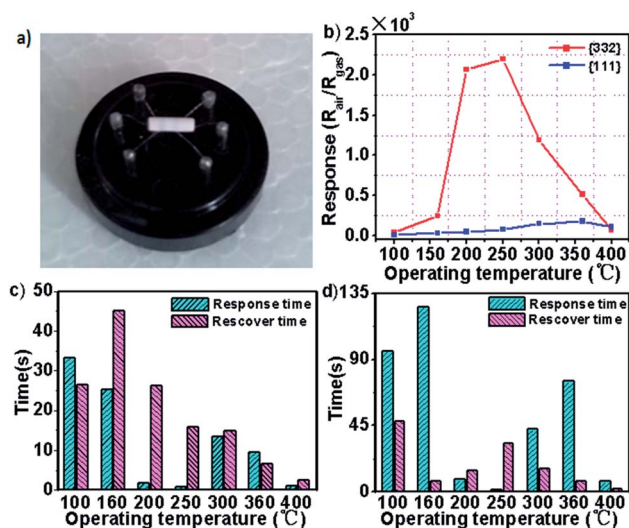

Fig. 3 (a) Typical TEM image of the octahedral SnO_2 {332} nanoparticle viewed along the [1$\bar{1}$0] direction; inset: the corresponding SEAD pattern. (b) Model of an ideal SnO_2 octahedron enclosed with {332} facets projected from the [1$\bar{1}$0] direction. (c) Typical TEM image of the octahedral SnO_2 {332} nanoparticle viewed along [$\bar{1}\bar{1}$3] direction; inset: the corresponding SEAD pattern. (d) Model of an ideal SnO_2 octahedron enclosed with {332} facets projected from the [$\bar{1}\bar{1}$3] direction.

Fig. 4 (a) A completed SnO_2 sensor. (b) The response of sensors based on SnO_2 {332} and {111} as a function of the operating temperature exposed to 800 ppm ethanol. The response and recovery time of (c) SnO_2 {111}-based sensor and (d) SnO_2 {332}-based sensor as a function of the operating temperature under an ethanol concentration of 800 ppm.

This journal is © The Royal Society of Chemistry 2014

J. Mater. Chem. A, 2014, **2**, 10623–10628 | **10625**

{332}-based sensor varies from 2 to 126 s (Fig. 4d). The change in response time of both the sensors is not a simple trend of increase or decrease as with an increasing temperature but all reach a minimum at temperature of 250 °C. The recovery times of both the sensors are all below 50 s with an increase in temperature. In summary, the ethanol-sensing performance of SnO$_2$ {332}-based sensor exhibits its best at 250 °C, whereas the response reaches a maximum value of 2200 to 800 ppm ethanol and the response duration reaches a minimum value of 1.5 s. In addition, for the SnO$_2$ {111}-based sensor, 360 °C is chosen as the optimal operating temperature, at which the sensor exhibits the highest response of 179 and the fastest response time of 9.5 s. The excellent ethanol-sensing performance with an ultrahigh response of the octahedral SnO$_2$ {332} is much better than the reported properties of the MoO$_3$,[19,20] Fe$_2$(MoO$_4$)$_3$@α-MoO$_3$ nanorods,[21] and ZnO$_2$.[22]

The typical response profiles of sensors based on SnO$_2$ {332} and {111} at optimum temperatures exposed to ethanol with different concentrations are shown in Fig. 5. With ethanol concentrations increasing from 5 to 800 ppm, the response of both the sensors continuously improves and presents a linear trend (inset of Fig. 5a and b). The response to the ethanol vapor of SnO$_2$ {111}-based sensor increases from 3.3 to 179 as ethanol concentrations increase, whereas the response of SnO$_2$ {332}-based sensor varies from 36.9 to 2200.

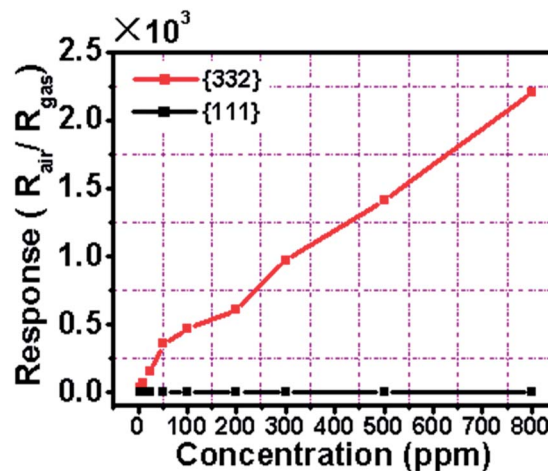To understand more about the difference in response between two kinds of sensors as the ethanol concentration

Fig. 6 The response of sensors based on SnO$_2$ {332} and {111} as a function of the ethanol concentration at optimum temperature.

changes, we compared the results in Fig. 5. As shown in Fig. 6, it can be clearly observed that the response of SnO$_2$ {332}-based sensor is always considerably higher than the SnO$_2$ {111}-based sensor, and has a faster growth trend under the ethanol concentration varying from 5 to 800 ppm. Fig. 7 shows the change of response and recovery time to various ethanol concentrations. The response time of SnO$_2$ {332}-based sensor
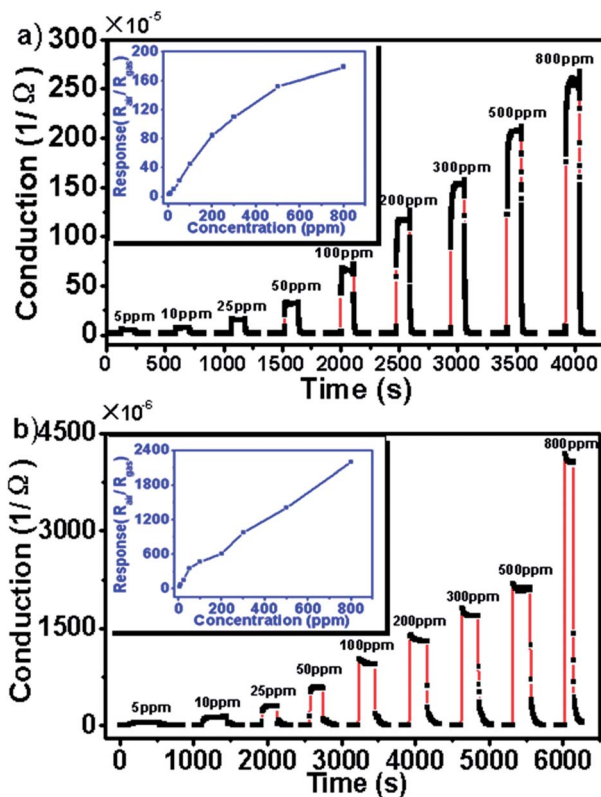

Fig. 5 Typical response profiles of (a) SnO$_2$ {111} sensor operating at 360 °C and (b) SnO$_2$ {332} sensor operating at 250 °C at different concentrations; inset: the corresponding response.
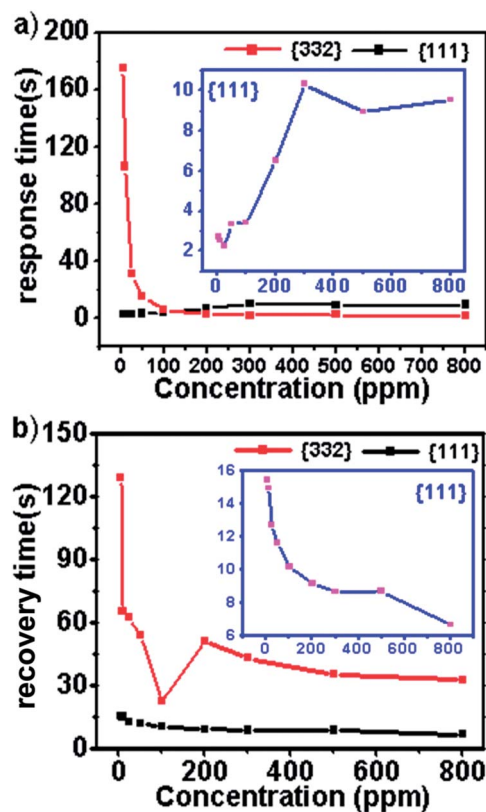

Fig. 7 The response time (a) and recovery time (b) of sensors made from SnO$_2$ {332} and {111} as a function of the ethanol concentration at optimum temperature; the insets are the time of SnO$_2$ {111}.

Table 1 Ethanol sensors based on SnO_2 materials reported before and in this work

Materials	Concentration (ppm)	Temperature (°C)	Response	Response time (s)	Recovery time (s)	Reference
SnO_2 nanoparticles	100	220	24.3	22	70	25
SnO_2 nanowires	100	400	11.8	4	30	14
SnO_2 nanowires mixed nanodendrites	100	360	31	—	—	15
SnO_2 nanotubes	100	200	<8	>40	<50	24
SnO_2 {111}	100	360	45.3	3.4	10.2	This work
SnO_2 {332}	100	250	464	5.8	22.8	This work

sharply drops to 6 s close to the response time of {111} as ethanol concentrations increased from 5 to 100 ppm and then slowly decreased to 1.5 s as the concentration sustainably grows to 800 ppm. Moreover, the response time of SnO_2 {111}-based sensor shows a generally increasing trend and is always below 11 s with an increase in ethanol concentration. As shown in Fig. 7b, the recovery time of the SnO_2 {332}-based sensor decreases sharply from 130 s to 23 s as ethanol concentration varies from 5 to 100 ppm similar to the trend of its response time, and still slowly decreases from 51 to 33 s as the concentration varies from 200 to 800 ppm. The recovery time of the SnO_2 {111}-based sensor is shorter than {332} under any ethanol concentration and decreases from 15.5 to 6.7 s.

The working principle of a typical resistive gas-sensor material, such as the SnO_2 sensor in this work, is based on a shift of the state of equilibrium of the surface-oxygen reaction because of the presence of the target analyte (receptor function). The resulting change in chemisorbed oxygen is recorded as a change in the resistance of the sensor material (transducer function).[23] The abovementioned response curves clearly indicated a sensing mechanism, which could be described as gas-surface chemisorption and electron acceptance, resulting in an increase in sensor conductivity. SnO_2 is an n-type wide band-gap semiconductor and its electronic conduction originates from point defects, which are either oxygen vacancies or foreign atoms acing as donors or acceptors.[24] In the ambient environment, SnO_2 nanocrystals are expected to adsorb both oxygen and moisture, in which moisture may be adsorbed as a hydroxyl group. Depending on the temperature, oxygen is ionosorbed on the surface predominantly as O^{2-} ions below 420 K or as O^- ions between 420–670 K.[23] The adsorbed O^{2-}/O^- and OH^- groups tap electrons from the conduction band of the SnO_2 nanocrystals, inducing the formation of a depletion layer on the surface of the SnO_2 nanocrystals. When exposed to ethanol vapor, the CH_3CH_2OH molecules are chemisorbed at the active sites on the surface of the SnO_2 nanocrystals. These ethanol molecules will be oxidized by the adsorbed oxygen and lattice oxygen (O^{2-}/O^-) of SnO_2 at the sensor-working temperature. During this oxidation process, electrons will transfer to the surface of SnO_2 nanocrystals to lower the number of trapped electrons, inducing a decrease in sensor resistance.

The SnO_2 {332}-based sensor shows improved ethanol-sensing performance than {111} because there are more dangling bonds on the {332} surface than on the {111} surface.[17,18] The response to the ethanol vapor of the SnO_2 {111}-based sensor is weaker compared with the SnO_2 {332}-based sensor; however, it is still much stronger than the SnO_2 nanostructures reported in the literature. Table 1 shows a comparison between the ethanol-sensing performances of the two sensors and literature reports. It is worth noting that the sensors prepared in this work exhibit improved sensing performances compared with the reported SnO_2 sensors. Under the same concentration of ethanol, the SnO_2 {111}-based sensor exhibits higher response (45.3) and faster response (3.4 s) and recovery times (10.2 s) than other sensors in Table 1. It also can be seen that the SnO_2 {332}-based sensor exhibits even better performance with high response of 464.

4   Conclusions

Both SnO_2 octahedral nanocrystals with exposed high-energy {111} and {332} facets synthesized by hydrothermal method exhibited high ethanol-sensing performance. The SnO_2 {332}-based sensor exhibited the highest response of 2200 to 800 ppm ethanol vapor at its optimum temperature of 250 °C, whereas the SnO_2 {111}-based sensor exhibited the highest response of 179 at its optimum temperature of 360 °C. The response time of the SnO_2 {332}-based sensor decreased from 175 to 1.5 s as the ethanol concentration varied from 5 to 800 ppm, whereas the response time of SnO_2 {111}-based sensor exhibited a general increasing trend, with the value always below 11 s. Correspondingly, the recovery time of the SnO_2 {332}-based sensor decreased sharply from 130 to 23 s as ethanol concentrations varied from 5 to 100 ppm, and still decreased slowly from 51 to 33 s, whereas the recovery time of the SnO_2 {111}-based sensor decreased from 15.5 to 6.7 s. Both the sensors based on SnO_2 {332} and {111} in this work showed excellent ethanol-sensing performances with high and fast responses and recovery times, compared with other materials reported, and the SnO_2 {332} exhibited even better properties than SnO_2 {111}.

References

1 S. Gubbala, V. Chakrapani, V. Kumar and M. K. Sunkara, *Adv. Funct. Mater.*, 2008, **18**, 2411–2418.

2 Y. J. Kim, K. H. Kim, P. Kang, H. J. Kim, Y. S. Choi and W. I. Lee, *Langmuir*, 2012, **28**, 10620–10626.

3 X. Hou, X. Wang, B. Liu, Q. Wang, Z. Wang, D. Chen and G. Shen, *ChemElectroChem*, 2014, **1**, 108–115.

4 H. Liu, S. Chen, G. Wang and S. Z. Qiao, *Chem. - Eur. J.*, 2013, **19**, 16897–16901.

5 P. Manjula, R. Boppella and S. V. Manorama, *ACS Appl. Mater. Interfaces*, 2012, **4**, 6252–6260.

6 S. Maeng, S. W. Kim, D. H. Lee, S. E. Moon, K. C. Kim and A. Maiti, *ACS Appl. Mater. Interfaces*, 2014, **6**, 357–363.

7 Y. Wang, H. C. Zeng and J. Y. Lee, *Adv. Mater.*, 2006, **18**, 645–649.

8 I. S. Hwang, J. K. Choi, H. S. Woo, S. J. Kim, S. Y. Jung, T. Y. Seong, I. D. Kim and J. H. Lee, *ACS Appl. Mater. Interfaces*, 2011, **3**, 3140–3145.

9 L. Hu, J. Yan, M. Liao, L. Wu and X. Fang, *Small*, 2011, **7**, 1012–1017.

10 O. Lupan, L. Chow, G. Chai, H. Heinrich, S. Park and A. Schulte, *Physica E*, 2009, **41**, 533–536.

11 Y. Li, Y. Guo, R. Tan, P. Cui, Y. Li and W. Song, *Mater. Lett.*, 2009, **63**, 2085–2088.

12 A. A. Firooz, A. R. Mahjoub and A. A. Khodadadi, *Sens. Actuators, B*, 2009, **141**, 89–96.

13 O. Lupan, L. Chow, G. Chai, A. Schulte, S. Park and H. Heinrich, *Mater. Sci. Eng., B*, 2009, **157**, 101–104.

14 N. Van Hieu, *Sens. Actuators, B*, 2010, **144**, 425–431.

15 S. Phadungdhitidhada, S. Thanasanvorakun, P. Mangkorntong, S. Choopun, N. Mangkorntong and D. Wongratanaphisan, *Curr. Appl. Phys.*, 2011, **11**, 1368–1373.

16 X. Han, M. Jin, S. Xie, Q. Kuang, Z. Jiang, Y. Jiang, Z. Xie and L. Zheng, *Angew. Chem.*, 2009, **48**, 9180–9183.

17 X. Wang, X. Han, S. Xie, Q. Kuang, Y. Jiang, S. Zhang, X. Mu, G. Chen, Z. Xie and L. Zheng, *Chem. - Eur. J.*, 2012, **18**, 2283–2289.

18 X. Han, L. Li and C. Wang, *Chem.–Asian J.*, 2012, **7**, 1572–1575.

19 D. Chen, M. Liu, L. Yin, T. Li, Z. Yang, X. Li, B. Fan, H. Wang, R. Zhang, Z. Li, H. Xu, H. Lu, D. Yang, J. Sun and L. Gao, *J. Mater. Chem.*, 2011, **21**, 9332.

20 L. Wang, P. Gao, D. Bao, Y. Chen, C. Chang, G. Li and P. Yang, *Cryst. Growth Des.*, 2014, **14**, 569–575.

21 Y. Chen, F. Meng, C. Ma, Z. Yang, C. Zhu, Q. Ouyang, P. Gao, J. Li and C. Sun, *J. Mater. Chem.*, 2012, **22**, 12900.

22 Y. Zeng, T. Zhang, L. Wang, R. Wang, W. Fu and H. Yang, *J. Phys. Chem. C*, 2009, **113**, 3442–3448.

23 M. E. Franke, T. J. Koplin and U. Simon, *Small*, 2006, **2**, 36–50.

24 G. X. Wang, J. S. Park, M. S. Park and X. L. Gou, *Sens. Actuators, B*, 2008, **131**, 313–317.

25 J. Zhang, S. Wang, Y. Wang, M. Xu, H. Xia, S. Zhang, W. Huang, X. Guo and S. Wu, *Sens. Actuators, B*, 2009, **139**, 369–374.

10628 | *J. Mater. Chem. A*, 2014, **2**, 10623–10628

This journal is © The Royal Society of Chemistry 2014